Journal of Sound and Vibration (1997) **206**(2), 243–260

DYNAMIC MODELLING OF ROTATING DRILLSTRINGS WITH BOREHOLE INTERACTIONS

A. P. Christoforou and A. S. Yigit

Department of Mechanical and Industrial Engineering, Kuwait University, P.O. Box 5969, *Safat* 13060, *Kuwait*

(*Received* 16 *December* 1996, *and in final form* 18 *April* 1997)

A dynamic model for the axial and transverse vibrations of a rotating drillstring is presented. The governing non-linear equations, which are obtained by using a Lagrangian approach, are fully coupled with time varying coefficients. They include the effects of gyroscopic moments, contact with the borehole wall, axial excitation due to bit/formation interactions, and hydrodynamic damping due to the presence of drilling mud outside the drillstring. Simulation results show that parametric resonance and whirling may occur simultaneously within the range of operating conditions of drilling. The dynamic behavior is quite complicated and may become non-periodic, suggesting a chaotic behavior.

1. INTRODUCTION

The Bottom Hole Assembly (BHA), which is the lower part of a drillstring used for drilling of oil and gas wells, is subject to severe vibrations caused by bit/formation and drillstring/borehole interactions. The drillstring vibration problem is fairly complex since it generally involves phenomena such as parametric resonance, whirling and contact with the borehole wall. The excessive lateral vibrations caused by such phenomena were observed to cause fatigue failure, wear and borehole enlargements [1].

Although there has been considerable research in the modelling and analysis of drillstring dynamics, a comprehensive understanding of all the vibration phenomena involved is still lacking [2, 3]. Furthermore, the complex and varying nature of the boundary conditions, and operational characteristics, undermine the utility of available models with respect to their predictive capabilities [4]. For this reason, the use of experimental drillstring measurement tools is currently the only reliable method for improving performance and solving real-time drilling problems. Theoretical studies on drillstring dynamics are still important, however, to improve the understanding of the various phenomena and thus provide better interpretation of experimental data [4].

Parametric instabilities caused by fluctuating weight on the bit were studied by Dunayevsky *et al*. [1]. They assumed the drillstring to be in permanent contact with the borehole wall along its entire length. The effects of transverse vibrations on the axial motion were also neglected. Shyu [5] studied extensively the bending vibrations of rotating and non-rotating drillstrings, where he investigated whirling and parametric instabilities. However, intermittent contact with the borehole wall was not addressed. A detailed study on whirling was carried out by Jansen [4, 6]: he included the effects of impact with the borehole wall. By using a lumped parameter model, he concluded that the resulting unstable drill collar motion could be periodic or chaotic. Berlioz *et al*. [3] investigated the

0022–460X/97/370243 + 18 $25.00/0/sv971091

lateral instabilities of drillstrings experimentally. They demonstrated that various types of instabilities, such as simple resonance, parametric resonance and combination resonance, may occur in a real drillstring. A finite element model was also developed.

Recently, the authors developed a non-linear model for a non-rotating drillstring, in which the full coupling between the transverse and axial motions was emphasized [7]. In the present study, the model proposed in reference [7] is extended for rotating drillstrings. In addition, parametric excitation due to bit/formation interactions as well as whirling due to unbalanced mass are considered. Also, non-linear damping is included by modelling the effects of mud outside the drillstring as hydrodynamic drag. Furthermore, the impact model is improved to accommodate oblique impacts and friction. The resulting governing equations are fully coupled and non-linear with time varying coefficients due to gyroscopic effects, axial shortening, intermittent contact with the borehole wall and hydrodynamic damping. The response to a harmonic axial bit load is obtained through numerical simulation.

2. DYNAMIC MODELLING

The BHA is modelled as shown in Figure 1. It is usually composed of drill collars (thick-walled tubulars) and stabilizers (coarsely grooved cylindrical elements of a larger diameter than the drill collars, that fit loosely in the borehole). The part of the lower portion of the drill collars supported by the stabilizers is under compression due to the weight of the upper portion of the drill collars. The compressive force applied at the bit is termed Weight-on-Bit (WOB) in the drilling literature and is essential for drilling. In this study, the lower portion of the drill collars is assumed to be under combined axial and lateral vibration, while the rest of the BHA is assumed to be undergoing only axial vibration. This assumption can be justified by noting that in most real applications the upper portion of the BHA is in permanent contact with the borehole wall. The transverse motion of the collars is confined by the borehole, and is assumed to be adequately modelled as a Rayleigh beam with simply supported boundary conditions at the stabilizer locations.

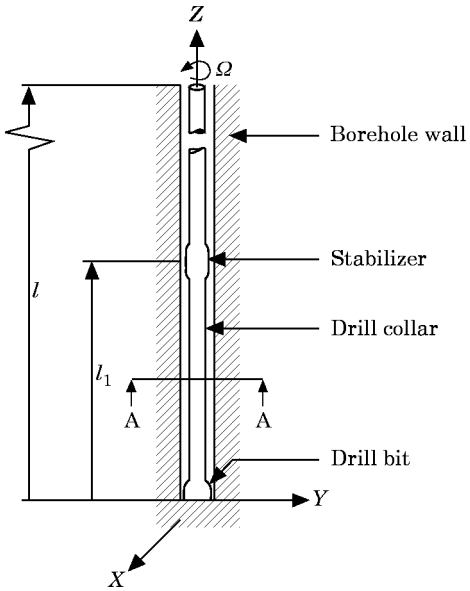

Figure 1. The sketch of the system.

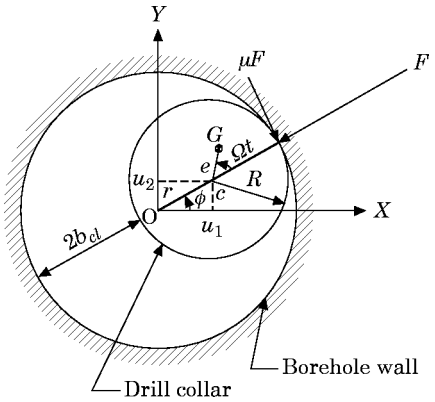

Figure 2. Section A–A through a borehole and deflected drill collar.

For the axial motion, the beam is assumed to be fixed at the bit and free at the end of the BHA.

The drillstring is assumed to be a solid cylinder of uniform cross-section rotating about the longitudinal z-axis with a constant angular speed Ω. The rotation of the drillstring undergoing transverse vibration results in gyroscopic moments which are included through external virtual work terms. The non-linear coupling between the axial and flexural deformations is retained by using finite strain measures. The equations of motion are obtained by using the assumed modes method and a Lagrangian approach. In this work, torsional vibrations are not considered.

2.1. KINETIC AND POTENTIAL ENERGY

For a rotating drillstring, the total kinetic energy can be written as

$$T = \tfrac{1}{2}\int_0^l \{\rho A V_G^2 + J_1\lambda_1^2 + J_2\lambda_2^2 + (J_1 + J_2)\lambda_3^2\}\,\mathrm{d}z, \tag{1}$$

where l is the total BHA length, ρ is the density of the material, and A is the cross-sectional area. V_G is the magnitude of the velocity of the mass center of a unit disk along the drillstring at a distance z. (Figure 2), which is given as

$$\mathbf{V}_G = (\dot{u}_1 - e\Omega\sin\Omega t)\mathbf{i} + (\dot{u}_2 + e\Omega\cos\Omega t)\mathbf{j} + \dot{u}_3\mathbf{k}, \tag{2}$$

where the u_i are the deflections in the x, y and z directions, respectively, e is the eccentricity of the center of mass with respect to the geometric center of the collars, **i**, **j** and **k** are the unit vectors along the x-, y- and z-axes, respectively, and $(\cdot)$ denotes a time derivative. J_1 and J_2 are the lateral mass moments of inertia per unit length with respect to the x-axis and y-axis, respectively, and for a symmetrical cross-section they are given by

$$J_1 = J_2 = \rho I, \tag{3}$$

where I is the area moment of inertia of the cross-section. The λ_i are the components of the angular velocity of the drillstring at distance z along the drillstring given as [8]

$$\lambda_1 = \dot{\psi}_1\cos\psi_2 - \dot{\theta}\cos\psi_1\sin\psi_2, \qquad \lambda_2 = \dot{\psi}_2 + \dot{\theta}\sin\psi_1,$$
$$\lambda_3 = \dot{\psi}_1\sin\psi_2 + \dot{\theta}\cos\psi_1\cos\psi_2. \tag{4–6}$$

where ψ_1 and ψ_2 are the rotations due to bending with respect to the x-axis and the y-axis, respectively, and $\dot{\theta} = \Omega = \text{constant}$, (i.e. no torsional deformation).

Assuming small angles, equations (4)–(6) are simplified to

$$\lambda_1 = \dot{\psi}_1 - \Omega\psi_2, \qquad \lambda_2 = \dot{\psi}_2 + \Omega\psi_1, \qquad \lambda_3 = \dot{\psi}_1\psi_2 + \Omega. \tag{7–9}$$

Substituting expressions (2), (3) and (7)–(9) into the kinetic energy, equation (1), and neglecting shear deformation, yields

$$T = \tfrac{1}{2}\int_0^l \{\rho A[(\dot{u}_1^2 + \dot{u}_2^2 + \dot{u}_3^2) + e^2\Omega^2 + 2e\Omega(\dot{u}_2\cos\Omega t - \dot{u}_1\sin\Omega t)]$$

$$+ \rho I[(\dot{u}_1')^2 + (\dot{u}_2')^2] + 2\rho I\Omega(\Omega - u_1'\dot{u}_2' - u_2'\dot{u}_1')\}\,\mathrm{d}z, \tag{10}$$

where $()'$ denotes a partial derivative with respect to z.

The strain energy due to axial and transverse deformations can be expressed as

$$U = \tfrac{1}{2}\int_0^l \{EI[(u_1'')^2 + (u_2'')^2] + EA[u_3' + \tfrac{1}{2}(u_1')^2 + \tfrac{1}{2}(u_2')^2]^2\}\,\mathrm{d}z, \tag{11}$$

where E is the Young's modulus. Note that in the above equation the non-linear axial strain is used to retain the coupling between the axial and transverse deflections.

2.2. VIRTUAL WORK

In order to complete the formulation, the virtual work done by external forces and gyroscopic moments is written as follows:

$$\delta W = \delta W_p + \delta W_f + \delta W_h + \delta W_g, \tag{12}$$

where δW_p, δW_f, δW_h and δW_g are the virtual work due to axial load P, contact, hydrodynamic damping and gyroscopic moments, respectively.

The virtual work due to the axial load is

$$\delta W_p = P\delta u_3(l_1). \tag{13}$$

The virtual work due to contact forces is

$$\delta W_f = \int_0^l \frac{F}{r}\{[u_1 + \text{sign}\,(\Phi)\mu u_2]\delta u_1 + [u_2 - \text{sign}\,(\Phi)\mu u_1]\delta u_2\}\delta(z - z_c)\,\mathrm{d}z, \tag{14}$$

where F is the impact force, $\delta(z - z_c)$ is the Dirac delta function, z_c being the impact location, r is the position of the geometric center of the cross-section along the drillstring (i.e., $r = \sqrt{u_1^2 + u_2^2}$), μ is the friction coefficient, and Φ is the velocity of the collar at the contact point, given as

$$\Phi = r_c\dot{\phi} + R\Omega, \tag{15}$$

where R is the outer radius of the drillstring, r_c is the position of the geometric center at the impact location and ϕ is given by

$$\phi = \tan^{-1}(u_2/u_1). \tag{16}$$

The impact force F is obtained from the Hertzian contact law as

$$F = \begin{cases} -\text{sign}\,(r_c) K_h (r - b_{cl})^{3/2}, & \text{if } |r_c| \geqslant b_{cl}, \\ 0, & \text{if } |r_c| < b_{cl}, \end{cases} \tag{17}$$

where K_h is the Hertzian stiffness, which can be obtained from the material properties and the contact geometry [9], and b_{cl} is the borehole clearance.

A damping force results from hydrodynamic drag and is modelled as a velocity squared proportional force in the direction opposite to the velocity of the collars [4]. The virtual work due to this force is

$$\delta W_h = -\rho_f C_D R \int_0^l \sqrt{\dot{u}_1^2 + \dot{u}_2^2}\,(\dot{u}_1 \delta u_1 + \dot{u}_2 \delta u_2)\,\mathrm{d}z, \tag{18}$$

where ρ_f is the density of the drilling mud and C_D is the hydrodynamic drag coefficient.

Whenever the axis about which a body is spinning is rotating about another axis, gyroscopic moments occur. For a rotating drillstring, gyroscopic moments result from the change in the angular momentum of the drillstring due to its bending motion. Because of the small angle assumption made in deriving the kinetic energy, these terms cannot be obtained from the kinetic energy and must be included via external work terms [8]. The virtual work due to gyroscopic moments can be written as

$$\delta W_g = 2\rho I \Omega \int_0^l (\dot{u}_2' \delta u_1 - \dot{u}_1' \delta u_2)\,\mathrm{d}z. \tag{19}$$

2.3. EQUATIONS OF MOTION

The governing equations can now be derived by using the assumed modes method. Due to the presence of the axial load acting at $z = l_1$, many modes will be necessary for convergence of axial deflections. One method to accelerate the convergence is to introduce forced modes [10]. In this case, this is achieved by adding one forced mode for the axial deformation in the modal expansions of the elastic deflections, given as

$$u_1(z, t) = \sum_{i=1}^{M} \phi_i(z) q_i(t), \qquad u_2(z, t) = \sum_{j=1}^{N} \phi_j(z) \eta_j(t), \tag{20, 21}$$

$$u_3(z, t) = \sum_{k=1}^{R} \beta_k(z) \gamma_k(t) + u_f(z, t), \tag{22}$$

where the $q_i(t)$, $\eta_j(t)$ and $\gamma_k(t)$ are unknown generalized co-ordinates, $\phi_i(z)$ and $\beta_k(z)$ are sets of admissible functions—that is, they satisfy the geometric boundary conditions [11] and $u_f(z, t)$ is the forced mode due to the axial load $P(t)$ acting at $z = l_1$, given as

$$u_f(z, t) = \begin{cases} \dfrac{P(t)}{EA} z, & \text{for } 0 \leqslant z \leqslant l_1, \\ \dfrac{P(t)}{EA} l_1, & \text{for } l_1 < z \leqslant l. \end{cases} \tag{23}$$

Here the $\phi_i(z)$ are selected as the normalized mode shapes of a simply supported beam in transverse motion, and the $\beta_k(z)$ are chosen as the normalized mode shapes for the fixed–free bar in axial motion; i.e.,

$$\phi_i(z) = \sqrt{\frac{2}{\rho A l_1}} \sin \frac{i\pi z}{l_1}, \qquad \beta_k(z) = \sqrt{\frac{2}{\rho A l}} \sin (2k-1)\frac{\pi z}{2l}. \tag{24, 25}$$

In this study, the BHA is assumed to be stabilized by a single stabilizer located at a distance l_1 from the bit. Note that while the support condition at the bit is very close to being simply supported, the actual support condition imposed by the stabilizer for the transverse motion of the lower portion of the beam is between simply supported and fixed. Thus, the above selection is only an approximation and is made on the basis of simplicity. A more realistic boundary condition will yield slightly different frequencies.

Substituting equations (20)–(22) into equations (10)–(12) and applying Lagrange's equations for q_i, η_j and γ_k yields the following non-linear coupled set of ordinary differential equations:

$$(1 + m_i^*)\ddot{q}_i + \omega_i^2 q_i + \sum_{j=1}^{N}\sum_{k=1}^{R} K_{ijk} q_j \gamma_k - 2G_i \Omega \dot{\eta}_i - S_i e \Omega^2 \cos \Omega t = Q_i, \qquad i = 1, 2, \ldots, M, \tag{26}$$

$$(1 + m_j^*)\ddot{\eta}_j + \omega_j^2 \eta_j + \sum_{i=1}^{M}\sum_{k=1}^{R} K_{ijk} \eta_i \gamma_k + 2G_j \Omega \dot{q}_j - S_j e \Omega^2 \sin \Omega t = \bar{Q}_j, \qquad j = 1, 2, \ldots, N, \tag{27}$$

$$\ddot{\gamma}_k + \bar{\omega}_k^2 \gamma_k + \tfrac{1}{2}\sum_{i=1}^{M}\sum_{j=1}^{N} K_{ijk}(q_i q_j + \eta_i \eta_j) + c_k \ddot{P} = 0, \qquad k = 1, 2, \ldots, R, \tag{28}$$

where ω_i and $\bar{\omega}_k$ are the characteristic frequencies for the transverse and the axial vibrations, respectively, and are given by

$$\omega_i^2 = \int_0^{l_1} EI(\phi_i'')^2 \, \mathrm{d}z + \int_0^{l_1} P(t)\,(\phi_i')^2 \, \mathrm{d}z, \tag{29}$$

$$\bar{\omega}_k^2 = \int_0^{l} EA(\beta_k')^2 \, \mathrm{d}z, \tag{30}$$

and m_i^*, K_{ijk}, G_i, S_i, c_k, Q_i and $\bar{Q}_j$ are obtained from the modal integrals as

$$m_i^* = \int_0^{l_1} \rho I(\phi_i')^2 \, \mathrm{d}z, \qquad K_{ijk} = \int_0^{l_1} EA\phi_i' \phi_j' \beta_k' \, \mathrm{d}z \tag{31, 32}$$

$$G_i = \int_0^{l_1} \rho I \phi_i \phi_i'' \, \mathrm{d}z, \qquad S_i = \int_0^{l_1} \rho A \phi_i \, \mathrm{d}z, \tag{33, 34}$$

$$c_k = \frac{\rho}{E}\left[\int_0^{l_1} \beta_k(z) z \, \mathrm{d}z + \int_{l_1}^{l} \beta_k(z) l_1 \, \mathrm{d}z\right], \tag{35}$$

TABLE 1

Parameters used in the simulations

Drillstring	Drilling mud
$E = 210$ GPa	$\rho_f = 1500$ kg/m^3
$\rho = 7860$ kg/m^3	$C_D = 1$
$R = 0{\cdot}1$ m	
$l = 200$ m	Contact
$l_1 = 20$ m	$K_h = 6.78 \times 10^{11}$ Nm$^{-1{\cdot}5}$
$e = 0{\cdot}005$ m	$\mu = 0{\cdot}1$
	$b_{cl} = 0{\cdot}05$ m
Weight on bit	
$P_0 = 100$ kN, $P_f = 50$ kN	

$$Q_i = \frac{F\left[\sum_{j=1}^{M} \phi_j(z_c)q_j + \sum_{j=1}^{N} \text{sign}\,(\Phi)\mu\phi_j(z_c)\eta_j\right]\phi_i(z_c)}{\sqrt{\left(\sum_{j=1}^{M} \phi_j(z_c)q_j\right)^2 + \left(\sum_{j=1}^{N} \phi_j(z_c)\eta_j\right)^2}}$$

$$- \int_0^{l_1} \rho_f C_D R \sqrt{\left(\sum_{j=1}^{M} \phi_j\dot{q}_j\right)^2 + \left(\sum_{j=1}^{N} \phi_j\dot{\eta}_j\right)^2}\left(\sum_{j=1}^{M} \phi_j\dot{q}_j\right)\phi_i \,\mathrm{d}z, \tag{36}$$

$$\bar{Q}_j = \frac{F\left[\sum_{i=1}^{N} \phi_i(z_c)\eta_i - \sum_{i=1}^{M} \text{sign}\,(\Phi)\mu\phi_i(z_c)q_i\right]\phi_j(z_c)}{\sqrt{\left(\sum_{i=1}^{M} \phi_i(z_c)q_i\right)^2 + \left(\sum_{i=1}^{N} \phi_i(z_c)\eta_i\right)^2}}$$

$$- \int_0^{l_1} \rho_f C_D R \sqrt{\left(\sum_{i=1}^{M} \phi_i\dot{q}_i\right)^2 + \left(\sum_{i=1}^{N} \phi_i\dot{\eta}_i\right)^2}\left(\sum_{i=1}^{N} \phi_i\dot{q}_i\right)\phi_j \,\mathrm{d}z. \tag{37}$$

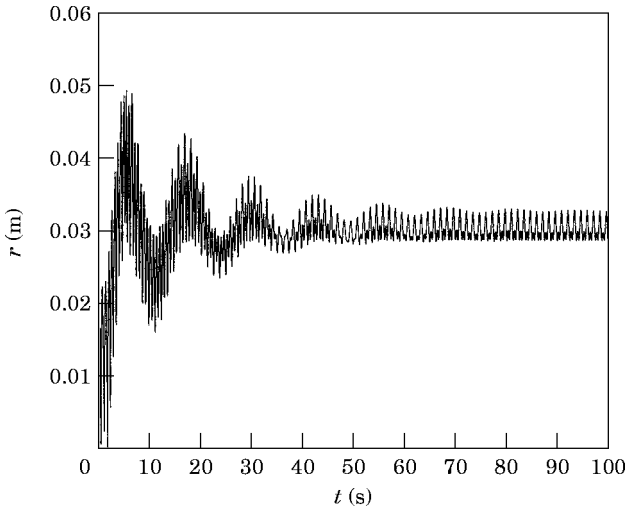

Figure 3. The radial deflection of the geometric center of the drill collar section ($\Omega = 5$ rad/s, $n = 1$).

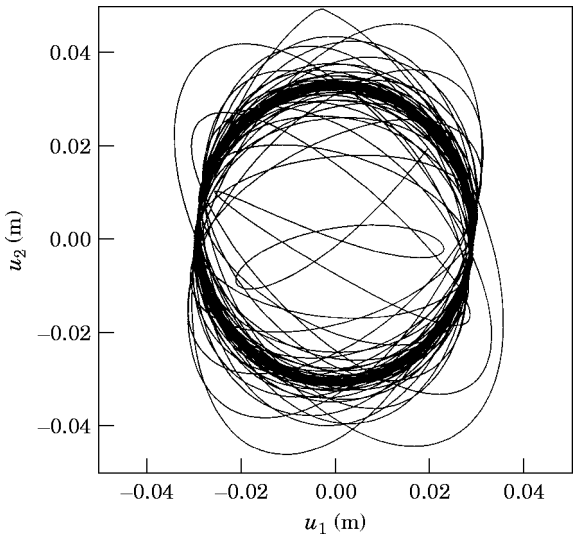

Figure 4. The trajectory of the geometric center of the drill collar section ($\Omega = 5$ rad/s, $n = 1$).

The axial excitation which represents WOB, and bit/formation interaction can be expressed as

$$-P(t) = P_0 + P_f \sin \omega_f t, \tag{38}$$

where P_0 is the static component of the WOB, and P_f and ω_f are the amplitude and the frequency of the fluctuating component of the WOB which results from the rotation of the drill bit. The frequency of this fluctuating component is related to the type of the bit

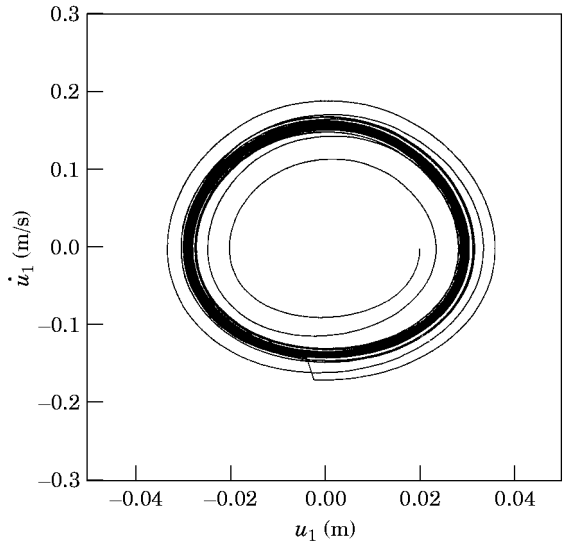

Figure 5. The phase plane for the transverse motion of the geometric center of the drill collar section ($\Omega = 5$ rad/s, $n = 1$).

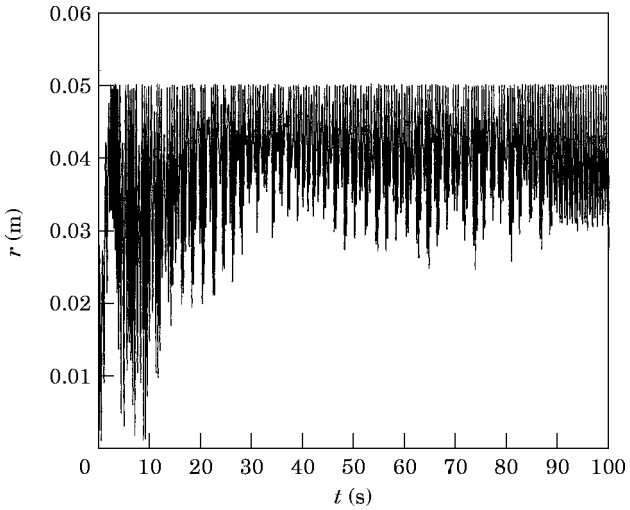

Figure 6. The radial deflection of the geometric center of the drill collar section ($\Omega = 6{\cdot}28$ rad/s, $n = 1$).

by $\omega_f = n\Omega$. For example, for a PDC (Polycrystalline Diamond Compact) bit, $n = 1$, and for a tricone bit $n = 3$ [1].

The governing equations are fully coupled non-linear differential equations with time varying coefficients. The axial and transverse motions are coupled due to non-linear elastic deflections, whereas the transverse motions in the x and y directions are coupled due to gyroscopic moments, hydrodynamic damping, impact and friction forces. The time varying coefficients are due to the axial excitation and axial–transverse coupling. The governing equations also contain harmonic excitations due to the axial force generated by the bit, and an out-of-balance mass (i.e., the eccentricity of the center of mass of the collar section with respect to its geometric center). These excitations introduce four types of vibration phenomena: simple resonance, where the axial forcing frequency, ω_f is roughly equal to the natural axial frequency, $\bar{\omega}_k$ [12]; parametric resonance, where the forcing frequency, ω_f

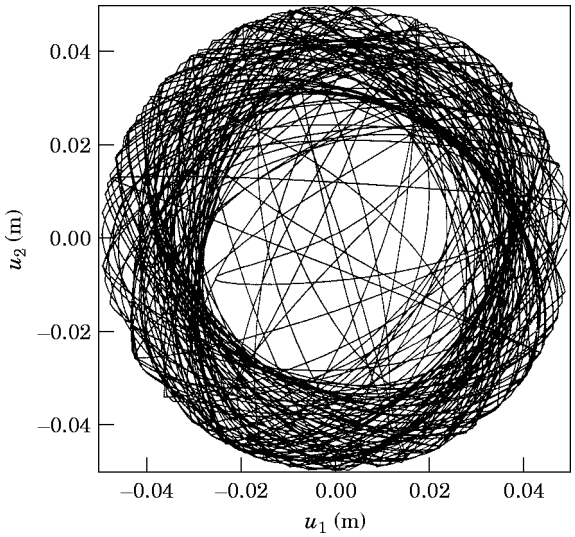

Figure 7. The trajectory of the geometric center of the drill collar section ($\Omega = 6{\cdot}28$ rad/s, $n = 1$).

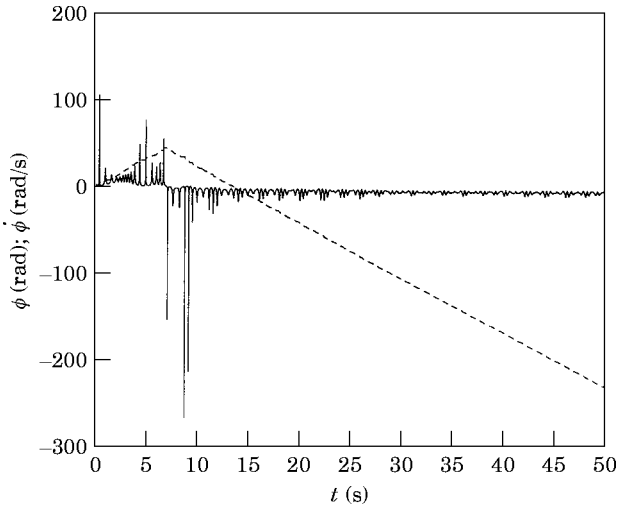

Figure 8. The angular motion of the drill collar section ($\Omega = 6{\cdot}28$ rad/s, $n = 1$); ——, ϕ; - - - -, $\dot{\phi}$.

is roughly twice the natural bending frequency, ω_i [1]; a combination resonance, where the sum of two bending frequencies is equal to an integer multiple of ω_f [3]; and a whirling resonance where the speed of rotation, Ω, is roughly equal to the natural bending frequency, ω_i [4]. Although a lot can be learned by studying each phenomenon separately, it is clear that all of the above-mentioned phenomena are coupled and may occur simultaneously. In what follows, the results of a set of simulations are presented to show the combined effects of these phenomena.

3. SIMULATION RESULTS AND DISCUSSION

A numerical solution procedure based on a variable-step variable order predictor–corrector differential equation solver is used to integrate the equations of motion [13]. As is well known, the accuracy of the numerical solution depends on the choice of the time step,

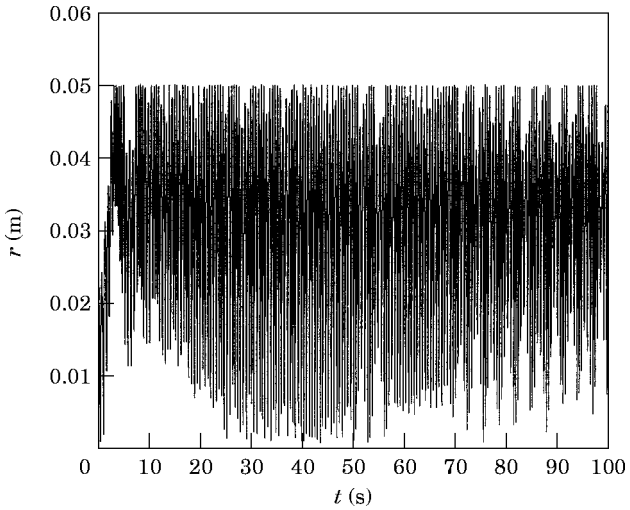

Figure 9. The radial deflection of the geometric center of the drill collar section ($\Omega = 5{\cdot}5$ rad/s, $n = 1$).

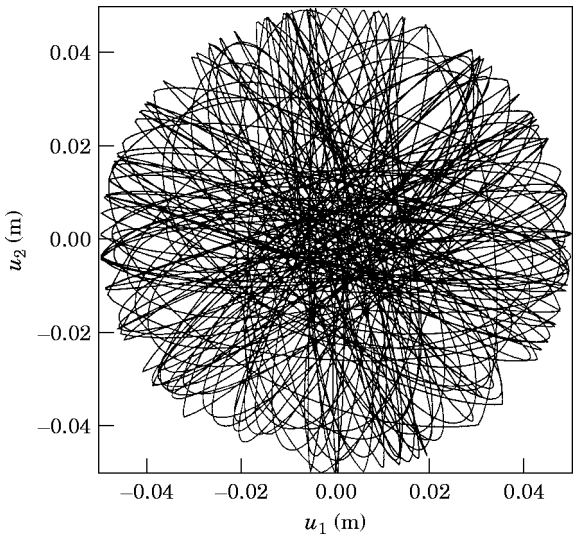

Figure 10. The trajectory of the geometric center of the drill collar section ($\Omega = 5{\cdot}5$ rad/s, $n = 1$).

which is problem dependent. The nominal time step used was 1/10 of the smallest natural period. In addition, the time step was reduced internally in the integrator to avoid discontinuities in the response, especially during impacts with the borehole wall. The time step is reduced by a factor of ten if the relative error bound specified (10^{-8}) is exceeded [13]. For the simulations given here, the time step varied between 0·1 ms and 0·0001 ms. Therefore, the numerical accuracy of the results is assured. The parameter values are chosen to represent cases close to those typically encountered in oilwell drilling, and are given in Table 1.

In the following simulations, one-mode approximations are used for the axial and transverse deformations. In addition, one forced mode is used for axial deformation to improve convergence. Clearly, the existence of impacts would require a multi-mode analysis, which will increase the dimension and complexity of the non-linear problem.

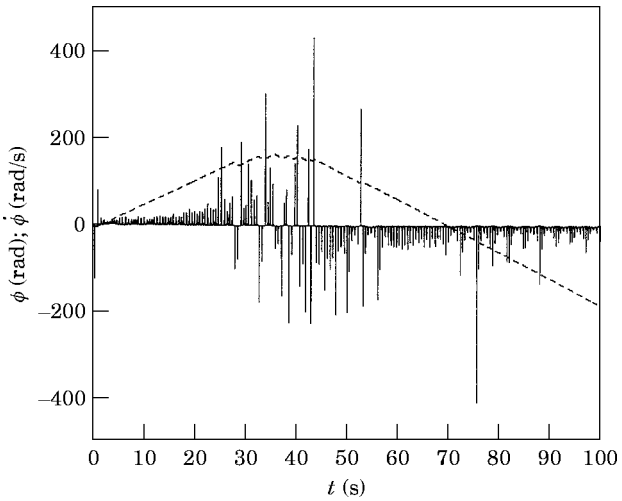

Figure 11. The angular motion of the drill collar section ($\Omega = 5{\cdot}5$ rad/s, $n = 1$); key as Figure 8.

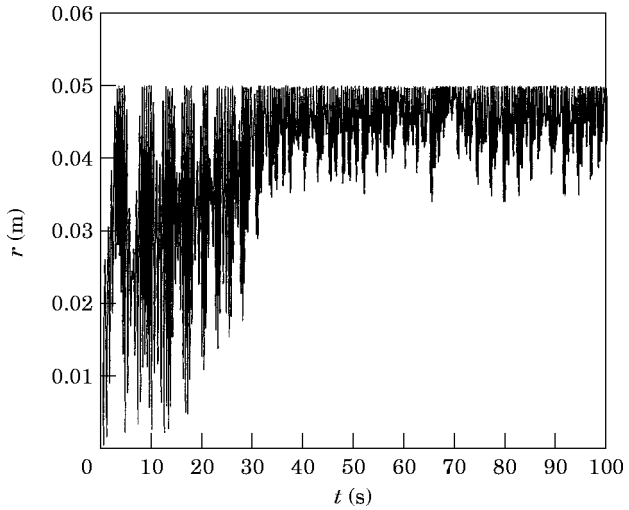

Figure 12. The radial deflection of the geometric center of the drill collar section ($\Omega = 5{\cdot}5$ rad/s, $n = 3$).

Since the objective of this work is to improve the understanding of the interactions between various phenomena such as whirling, parametric excitation and non-linear coupling, one-mode approximations for the deformations are deemed to be adequate. For a real BHA configuration, however, the results should only be interpreted in a qualitative sense. It should also be noted that the one-mode approximation used for the transverse motion also simplifies the contact condition in that the impact always occurs at the mid-span of the last drill collar section.

A set of simulations were carried out with the bit factor, $n = 1$. In this case, the forcing frequency, ω_f, is equal to the rotating speed Ω, and the critical whirling speed, estimated from equation (29) is 5·5 rad/s. The dynamic response when the rotating speed $\Omega = 5$ rad/s is shown in Figures 3–5. Note that the rotating speed is close to the critical whirling speed and consequently the amplitudes of vibration will be large. Indeed, as can be seen from

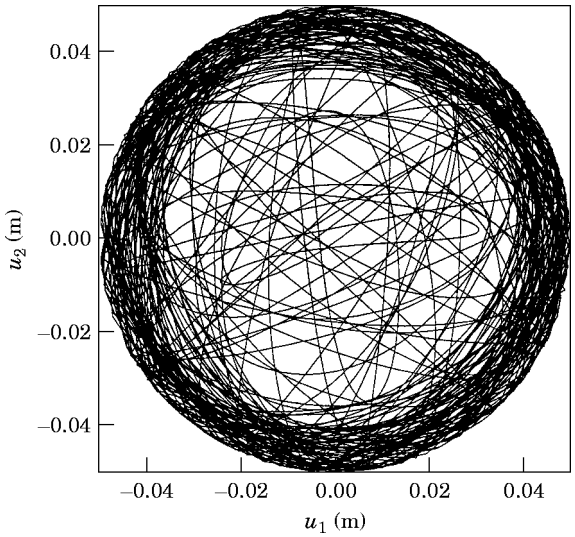

Figure 13. The trajectory of the geometric center of the drill collar section ($\Omega = 5{\cdot}5$ rad/s, $n = 3$).

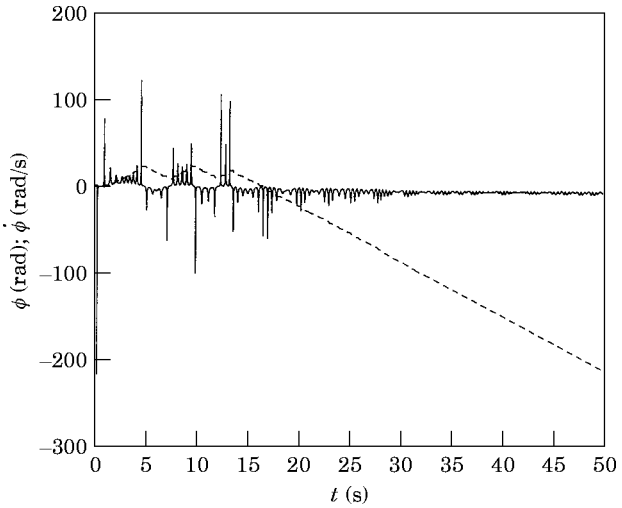

Figure 14. The angular motion of the drill collar section ($\Omega = 5{\cdot}5$ rad/s, $n = 3$); key as Figure 8.

Figures 3 and 4, the amplitudes larger than the borehole clearance cause impacts with the borehole wall. Because of the presence of dissipative effects such as friction and hydrodynamic damping, the vibrations eventually settle into a limit cycle behavior. This is clearly seen in the phase plane given in Figure 5. Overall, the drillstring behavior is similar to a forward whirl with constant speed ($\dot{\phi} = \Omega$).

When the rotating speed is increased to $\Omega = 6{\cdot}28$ rad/s, the steady state whirling amplitude is higher, which results in continuous impacts with the borehole wall as illustrated in Figures 6 and 7. In Figure 8 it is shown that, for the time period covered by the simulation, the drillstring experiences both forward and backward whirl. It seems that after the large amplitude transient the motion becomes periodic with a larger amplitude than that of the previous case.

In Figures 9–11 is shown the dynamic behavior when the rotating speed is equal to the estimated critical whirling speed, $\Omega = 5{\cdot}5$ rad/s. As expected, the whirling amplitudes are

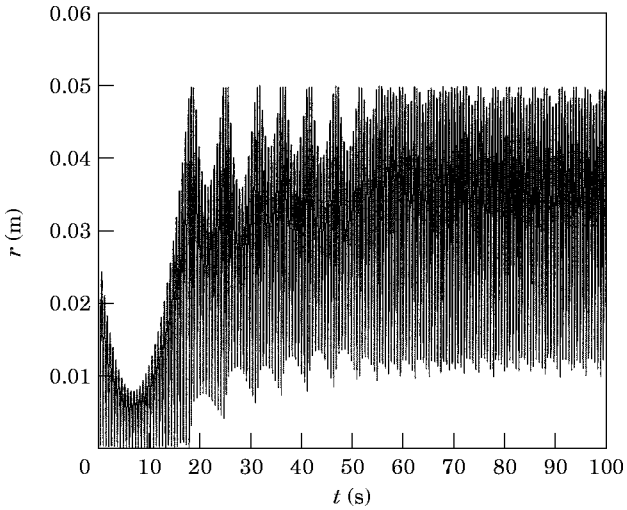

Figure 15. The radial deflection of the geometric center of the drill collar section ($e = 0$, $\Omega = 3{\cdot}67$ rad/s, $n = 3$).

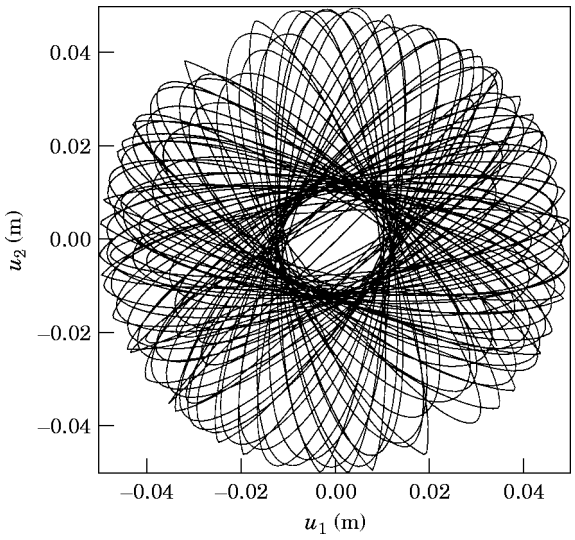

Figure 16. The trajectory of the geometric center of the drill collar section ($e = 0$, $\Omega = 3{\cdot}67$ rad/s, $n = 3$).

larger than those of the previous cases (see Figure 9). As clearly seen in Figure 10, this is a highly irregular whirling motion. More information about the whirling behavior can be obtained by observing the angular rotation ϕ, and whirling speed $\dot{\phi}$, shown in Figure 11. For the time period covered by the simulation, the initial forward whirl changes into a transitory phase, in which the whirl direction continuously changes between forward and backward, and eventually settles into a backward whirl with a constant average whirl speed which is close to the effective bending frequency [4].

For the next set of simulations the forcing frequency, ω_f, is assumed to be three times the rotating speed, Ω (i.e., $n = 3$). In Figures 12–14 is shown the response when the rotating speed, $\Omega = 5{\cdot}5$ rad/s, which again coincides with the estimated critical whirling speed. A

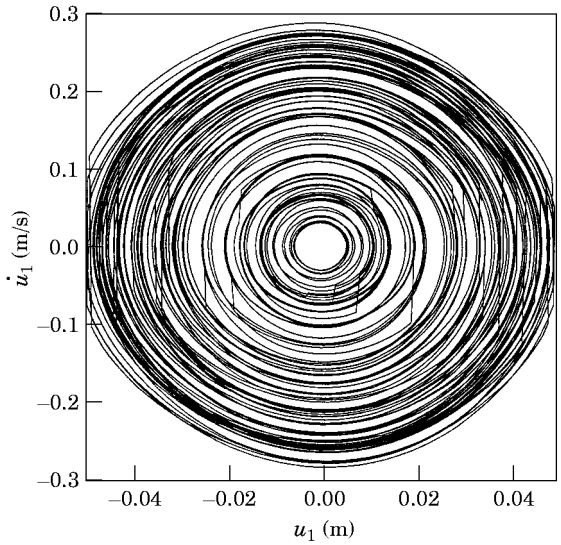

Figure 17. The phase plane for the transverse motion of the geometric center of the drill collar section ($e = 0$, $\Omega = 3{\cdot}67$ rad/s, $n = 3$).

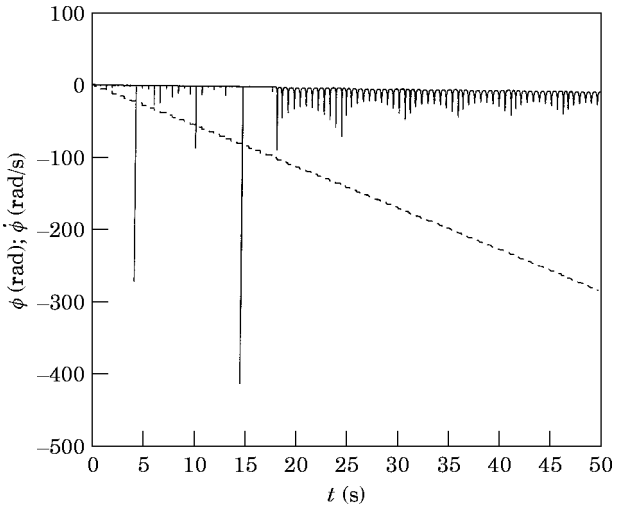

Figure 18. The angular motion of the drill collar section ($e = 0$, $\Omega = 3{\cdot}67$ rad/s, $n = 3$); key as Figure 8.

comparison of Figures 9 and 12 reveals that the higher excitation frequency results in a lower fluctuating component in the drillstring deflection amplitude. As can be seen in Figure 14, the drillstring, after an initial transient, goes into backward whirling and stays close to the borehole wall (compare Figures 12 and 13 with Figures 9 and 10).

In order to investigate the effect of parametric resonance alone, the excitation frequency is taken to be equal to twice the effective bending frequency (i.e., $\omega_f = 11$ rad/s), and the eccentricity is assumed to be zero to eliminate the excitation due to unbalance. Since $n = 3$, the corresponding rotating speed is $\Omega = 3{\cdot}667$ rad/s. As expected in Figures 15–17 is shown behavior typical of parametric instability. As can be seen in Figure 18, the motion is a backward whirl with a constant average speed. The results with a non-zero eccentricity are shown in Figures 19–22. The result of the excitation due to unbalance is a strongly irregular motion, as seen in Figure 20. The combined effect of whirling and parametric excitation can clearly be seen by comparing the results of the last two simulations.

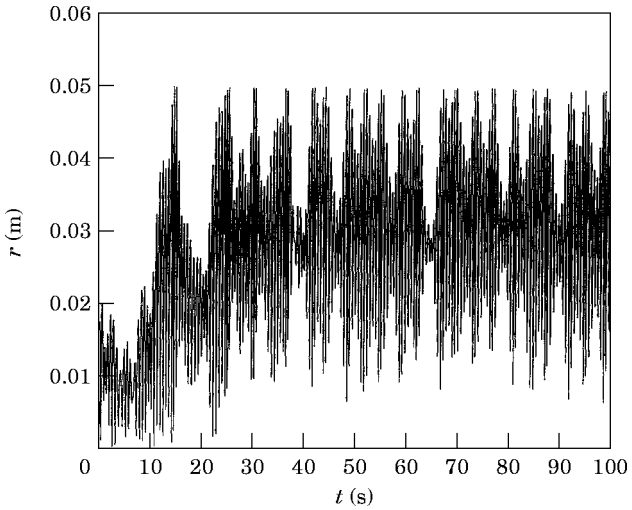

Figure 19. The radial deflection of the geometric center of the drill section ($\Omega = 3{\cdot}67$ rad/s, $n = 3$).

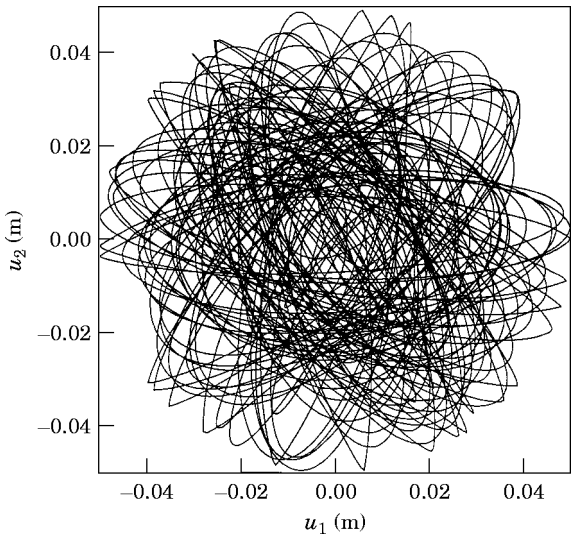

Figure 20. The trajectory of the geometric center of the drill collar section ($\Omega = 3{\cdot}67$ rad/s, $n = 3$).

Although the overall amplitudes are similar, they appear to be modulated due to the effect of unbalance (see Figure 19), and consequently the number of impacts is reduced. Despite the difference in the transient, the average whirling speeds are the same for both cases.

The above simulation results qualitatively confirm some of the field observations reported by Vandiver *et al*. [2]. By inspecting bending moment and phase angle time histories, they were able to detect the presence of forward and backward whirling and/or impacts with the borehole wall. Parametric coupling was also cited among possible causes of such vibrations. As mentioned earlier, experimental results [3] also confirm the existence of similar behavior. Thus, the proposed dynamic model is capable of predicting the actual dynamic behavior of drillstrings in a qualitative manner. The quantitative behavior,

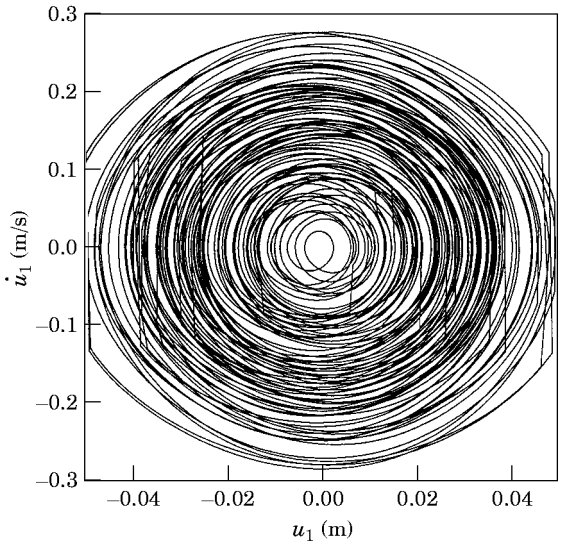

Figure 21. The phase plane for the transverse motion of the geometric center of the drill collar section ($\Omega = 3{\cdot}67$ rad/s, $n = 3$).

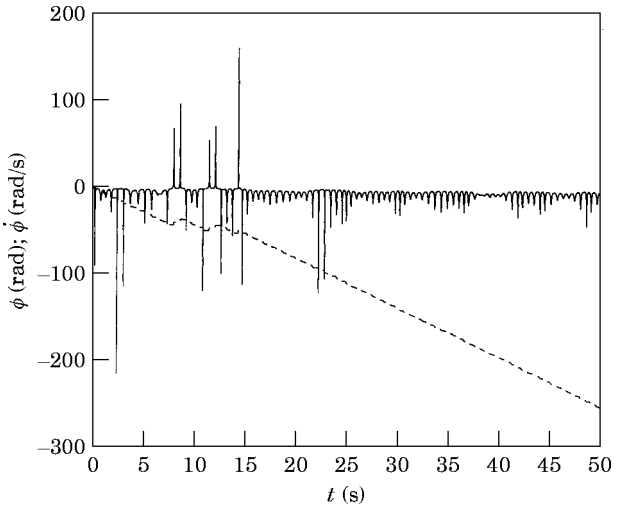

Figure 22. The angular motion of the drill collar section ($\Omega = 3{\cdot}67$ rad/s, $n = 3$); key as Figure 8.

however, depends on the actual values of the model parameters such as borehole friction, hydrodynamic damping and contact stiffness, which vary significantly during operation. In most cases, the values of these parameters are very difficult to obtain. Although it may be useful to study their effects on the dynamic behavior, a detailed parametric study is beyond the scope of this paper.

4. CONCLUSIONS

A dynamic model of the coupled axial and transverse vibrations of a rotating drillstring has been presented. The model includes gyroscopic moments, contact with the borehole wall, axial excitation due to bit/formation interactions, and hydrodynamic damping due to the presence of drilling mud outside the drillstring. The dynamic behavior is governed by a system of fully coupled non-linear equations with time varying coefficients. The governing equations are solved numerically for various sets of parameter values. The well known phenomena of parametric resonance and whirling, which cause violent lateral vibrations, are shown to occur simultaneously within the range of operating conditions of drilling.

Because of the non-linear and time varying nature of the terms in the governing equations, the dynamic behavior is quite complicated and may become non-periodic, suggesting chaotic behavior. Further analytical and numerical studies are needed, however, to improve the understanding of the associated non-linear phenomena.

ACKNOWLEDGMENT

This work was supported by Kuwait University, Research Administration, Grant Number EM-075.

REFERENCES

1. V. A. Dunayevsky, F. Abbassian and A. Judzis 1993 *Society of Petroleum Engineers*, *Drilling and Completion* **8**, 84–92. Dynamic stability of drillstrings under fluctuating weight on bit.

2. J. K. Vandiver, J. W. Nicholson and R. J. Shyu *Society of Petroleum Engineers Drilling Engineering* **5**, 282–190. Case studies of the bending vibration and whirling motion of drill collars.
3. A. Berlioz, J. Der Hogopian, R. Dufour and E. Draoui 1996 *Transactions of the American Society of Mechanical Engineers*, *Journal of Vibration and Acoustics* **118**, 292–298. Dynamic behavior of a drillstring: experimental investigation of lateral instabilities.
4. J. D. Jansen 1991 *Journal of Sound and Vibration* **147**, 115–135. Non-linear rotor dynamics as applied to oilwell drillstring vibrations.
5. R. J. Shyu 1989 *PhD Dissertation*, *Massachusetts Institute of Technology*, *Department of Ocean Engineering*, *Cambridge*. Bending vibrations of rotating drillstrings.
6. J. D. Jansen 1992 *Society of petroleum Engineers*, *Drilling Engineering* **7**, 107–114. Whirl and chaotic motion of stabilized drill collars.
7. A. S. Yigit and A. P. Christoforou 1996 *Journal of Sound and Vibration* **195**, 617–627. Coupled axial and transverse vibrations of oilwell drillstrings.
8. S. H. Choi, C. Pierre and A. G. Ulsoy 1992 *Transactions of the American Society of Mechanical Engineers*, *Journal of Vibration and Acoustics* **114**, 249–259. Consistent modeling of rotating Timoshenko shafts subject to axial loads.
9. W. Goldsmith 1960 *Impact*. London: Edward Arnold.
10. K. Gu and B. H. Tongue 1987 *Transactions of the American Society of Mechanical Engineers*, *Journal of Applied Mechanics* **54**, 904–909. A method to improve the modal convergence for structures with external forcing.
11. L. Meirovitch 1967 *Analytical Methods in Vibrations*. New York: Macmillan.
12. P. R. Paslay and D. B. Bogy 1963 *Transactions of the American Society of Mechanical Engineers*, *Journal of Engineering for Industry* **May**, 187–194. Drill string vibrations due to intermittent contact of bit teeth.
13. G. D. Byrne and A. C. Hindmarsh 1975 *ACM Transactions on Mathematical Software* **1**, 71–76. A polyalgorithm for the numerical solution of ordinary differential equations